Adjoint consistency analysis of residual-based variational multiscale methods[☆]

J.E. Hicken[a,1,*], J. Li[a,3], O. Sahni[a,1], A.A. Oberai[a,2]

[a] *Department of Mechanical, Aerospace, and Nuclear Engineering, Rensselaer Polytechnic Institute, Troy, New York, United States*

Abstract

We investigate the conditions under which residual-based variational multiscale methods are adjoint, or dual, consistent for model hyperbolic and elliptic partial differential equations. In particular, while many residual-based variational multiscale stabilizations are adjoint consistent for hyperbolic problems and finite-element spaces, only a few are adjoint consistent for elliptic problems.

Keywords: dual consistency, adjoint consistency, variational multiscale method, functional superconvergence, differentiate-then-discretize, discretize-then-differentiate

1. Introduction

Adjoint variables arise in many applications, including output-based error estimation and adaptation, inverse problems, and optimization. The equations governing the adjoint variables are typically obtained using either the differentiate-then-discretize approach or the discretize-then-differentiate approach [1]. In the former, the adjoint PDE is derived first and then discretized, while in the latter, the primal PDE and functional are discretized and the adjoint linear system follows from differentiation of the algebraic equation.

We say the primal problem is dual, or adjoint, consistent if the discretize-then-differentiate approach leads to a linear system that is equivalent to a consistent discretization of the adjoint PDE. Discretizations that are adjoint consistent have been shown to enjoy certain advantages over discretizations that are adjoint inconsistent.

- Adjoint consistency leads to optimal error estimates in the L^2 norm [2].
- Integral functionals are superconvergent relative to the solution error [3, 4]. This is valuable from an efficiency perspective, since, for the same number of nodes, an adjoint-consistent for-

[☆]This work was supported by Rensselaer Polytechnic Institute

[*]corresponding author

Email addresses: hickej2@rpi.edu (J.E. Hicken), lij14@rpi.edu (J. Li), sahni@rpi.edu (O. Sahni), oberaa@rpi.edu (A.A. Oberai)

[1]Assistant Professor

[2]Professor

[3]Graduate Student

mulation may have a significantly smaller functional error. The numerical examples presented in Section 5 illustrate this.

- Similarly, functional gradients computed using the adjoint variables are superconvergent. In addition, gradients computed in this fashion are equivalent, within machine precision, to sensitivities computed using algorithmic differentiation [5]. This equivalence is important when using conventional optimization algorithms that expect the user to supply accurate gradients.

- A posteriori output error estimates based on adjoint consistent schemes — or schemes that are asymptotically adjoint consistent — exhibit better effectivity [6].

Given these advantages, there has been significant interest in studying the adjoint consistency of various discretizations [2, 4, 7–10]. In this paper, we investigate the adjoint consistency of variational-multiscale methods [11–19]. In particular, we focus on residual-based variational multiscale stabilization (RBVMS) and establish conditions under which this form of stabilization leads to adjoint consistency.

2. Adjoint consistency analysis

We begin by reviewing the concept of adjoint, or dual, consistency [2, 4, 20]. Consider the following variational problem corresponding to the weak form of a partial differential equation (PDE) on the domain $\Omega \subset \mathbb{R}^d$: find $u \in \mathsf{V}$ such that

$$\mathcal{R}(v, u) = 0, \qquad \forall v \in \mathsf{V}, \tag{1}$$

where V denotes an appropriate Hilbert space on the domain Ω, and $\mathcal{R} : \mathsf{V} \times \mathsf{V} \to \mathbb{R}$ is a semilinear form (linear in the first argument). In addition, suppose we are interested in nonlinear integral functionals $\mathcal{J} : \mathsf{V} \to \mathbb{R}$ that depend on the solution to (1); for example, when $\mathcal{R}$ corresponds to the weak form of the Navier-Stokes equations, $\mathcal{J}$ might be the lift or drag force.

To find the dual problem corresponding to the functional $\mathcal{J}$ and primal variational problem (1), we introduce the Lagrangian,

$$\mathcal{L}(\psi, u) \equiv \mathcal{J}(u) + \mathcal{R}(\psi, u), \tag{2}$$

where $\psi \in \mathsf{V}$. We arrive at the dual problem by finding ψ such that variations in $\mathcal{L}$ about u vanish:

$$\delta\mathcal{L} \equiv \mathcal{L}'[u](\psi, \delta u) = \mathcal{J}'[u](\delta u) + \mathcal{R}'[u](\psi, \delta u) = 0, \quad \forall \delta u \in \mathsf{V},$$

or, equivalently

$$\mathcal{J}'[u](v) + \mathcal{R}'[u](\psi, v) = 0, \quad \forall v \in \mathsf{V}, \tag{3}$$

where the prime indicates (Fréchet) linearization with respect to the term in square brackets.

We now turn to the finite-dimensional case and introduce V^h, a space that approximates V. Then, the discretization of the primal variational equation (1) leads to the following problem: find $u^h \in \mathsf{V}^h$ such that

$$\mathcal{R}_h(v^h, u^h) = 0, \qquad \forall v^h \in \mathsf{V}^h. \tag{4}$$

The subscript h on $\mathcal{R}_h$ indicates that operators in the discretized semilinear form may depend on the discrete solution u^h in the nonlinear case. The discretized functional will be denoted by $\mathcal{J}_h : \mathsf{V}^h \to \mathbb{R}$. Note that in general, $\mathcal{R}_h$ and $\mathcal{R}$, and $\mathcal{J}_h$ and $\mathcal{J}$, are not the same.

The analysis used to derive the adjoint variational problem can be applied to the finite-dimensional case. This leads to the following linear system that is satisfied by the discrete adjoint variable $\psi^h \in \mathsf{V}^h$:

$$\mathcal{J}_h'[u^h](v^h) + \mathcal{R}_h'[u^h](\psi^h, v^h) = 0, \qquad \forall v^h \in \mathsf{V}^h. \tag{5}$$

Adjoint consistency arises from the relationship between the discrete adjoint variational equation (5) and the infinite-dimensional adjoint solution ψ. For completeness, we include the definition of adjoint consistency below; see, for example, [4].

Definition 1 (Dual/Adjoint Consistency). The finite element discretization (4) and discrete functional $\mathcal{J}_h$ are dual consistent if

$$\mathcal{J}_h'[u](v^h) + \mathcal{R}_h'[u](\psi, v^h) = 0, \qquad \forall v^h \in \mathsf{V}^h, \tag{6}$$

where u and ψ are weak solutions to the primal, (1), and adjoint, (3), variational equations, respectively.

In the absence of boundary conditions and stabilization, it is easy to see that a Galerkin finite-element discretization is dual consistent. Adjoint consistency is less clear when stabilization is present. For example, is dual consistency preserved when a residual-based variational multiscale stabilization is introduced in (4)? This is the question we now consider for first- and second-order PDEs.

3. First-order System of PDEs

We begin by examining the adjoint consistency of a hyperbolic system of m PDEs discretized by the variational multiscale method, e.g. the Euler equations that model inviscid compressible flows. To simplify the analysis, we assume that all incoming characteristics enter through the boundary $\Gamma_{\text{in}} \subset \Gamma$. The outlet boundary is given by $\Gamma_{\text{out}} \equiv \Gamma \setminus \Gamma_{\text{in}}$. Then, the strong form of our nonlinear hyperbolic system is

$$\begin{aligned} \boldsymbol{\mathcal{N}}(\mathbf{u}) \equiv \boldsymbol{\mathcal{F}}_{i,i}(\mathbf{u}) &= \mathbf{0}, \qquad \forall \boldsymbol{x} \in \Omega, \\ \mathbf{u} &= \mathbf{u}_{\text{in}}, \qquad \forall \boldsymbol{x} \in \Gamma_{\text{in}}, \end{aligned} \tag{7}$$

where $\boldsymbol{\mathcal{N}}(\mathbf{u})$ is the residual and $\{\boldsymbol{\mathcal{F}}_i\}_{i=1}^d$ are the spatial components of the flux vector. Partial derivatives are denoted $\mathbf{u}_{,i} = \partial \mathbf{u}/\partial x_i$ and the Einstein summation convention is adopted. The weak form of (7) is, find $\mathbf{u} \in [\mathsf{V}]^m \equiv \{v_k \in \mathsf{V}, k = 1, \ldots, m\}$ such that

$$\mathcal{R}(\mathbf{v}, \mathbf{u}) \equiv -\int_\Omega \mathbf{v}_{,j}^T \boldsymbol{\mathcal{F}}_j(\mathbf{u})\, d\Omega + \int_{\Gamma_{\text{out}}} \mathbf{v}^T \boldsymbol{\mathcal{F}}_j(\mathbf{u}) \hat{n}_j\, d\Gamma + \int_{\Gamma_{\text{in}}} \mathbf{v}^T \boldsymbol{\mathcal{F}}_j(\mathbf{u}_{\text{in}}) \hat{n}_j\, d\Gamma = 0, \qquad \forall \mathbf{v} \in [\mathsf{V}]^m, \tag{8}$$

where $\hat{\mathbf{n}}$ denotes the outward-pointing unit normal on Γ and $\mathsf{V} \equiv H^1(\Omega)$.

To define the dual problem, we introduce a functional of the form

$$\mathcal{J}(\mathbf{u}) \equiv \int_\Omega \mathcal{G}(\mathbf{u}, \nabla \mathbf{u})\, d\Omega. \tag{9}$$

As a concrete example, $\mathcal{J}(\mathbf{u})$ might be the total kinetic energy in a flow field when $\mathbf{u}$ is governed by the Euler equations. For compatibility with the hyperbolic adjoint equation derived below, we assume[4]

$$\mathcal{G}'[\mathbf{u}_{,j}]\hat{n}_j = 0, \qquad \forall \boldsymbol{x} \in \Gamma_{\text{in}}. \tag{10}$$

Without this compatibility condition, the adjoint boundary conditions would be over specified.

The weak form of the adjoint PDE follows by substituting (8) and (9) into (3): find $\boldsymbol{\psi} \in [\mathsf{V}]^m$ such that

$$\begin{aligned}\mathcal{J}'[\mathbf{u}](\mathbf{v}) + \mathcal{R}'[\mathbf{u}](\boldsymbol{\psi}, \mathbf{v}) \equiv \int_\Omega \mathcal{G}'[\mathbf{u}]\mathbf{v}\, d\Omega + \int_\Omega \mathcal{G}'[\mathbf{u}_{,j}]\mathbf{v}_{,j}\, d\Omega - \int_\Omega \boldsymbol{\psi}_{,j}^T \boldsymbol{\mathcal{F}}_j'[\mathbf{u}]\mathbf{v}\, d\Omega \\ + \int_{\Gamma_{\text{out}}} \boldsymbol{\psi}^T \boldsymbol{\mathcal{F}}_j'[\mathbf{u}]\hat{n}_j \mathbf{v}\, d\Gamma = 0, \qquad \forall \mathbf{v} \in [\mathsf{V}]^m.\end{aligned} \tag{11}$$

Assuming a sufficiently smooth primal solution, we can rewrite the adjoint variational problem (11) by integrating by parts on the $\mathbf{v}_{,j}$ term, and making use of the compatibility condition (10):

$$\begin{aligned}\mathcal{J}'[\mathbf{u}](\mathbf{v}) + \mathcal{R}'[\mathbf{u}](\boldsymbol{\psi}, \mathbf{v}) \equiv \int_\Omega \left\{ \mathcal{G}'[\mathbf{u}] - \left(\mathcal{G}'[\mathbf{u}_{,j}]\right)_{,j} - \boldsymbol{\psi}_{,j}^T \boldsymbol{\mathcal{F}}_j'[\mathbf{u}] \right\} \mathbf{v}\, d\Omega \\ + \int_{\Gamma_{\text{out}}} \left\{ \boldsymbol{\psi}^T \boldsymbol{\mathcal{F}}_j'[\mathbf{u}]\hat{n}_j + \mathcal{G}'[\mathbf{u}_{,j}]\hat{n}_j \right\} \mathbf{v}\, d\Gamma = 0, \qquad \forall \mathbf{v} \in [\mathsf{V}]^m.\end{aligned} \tag{12}$$

We can extract the strong form of the adjoint PDE by inspecting the above variational form. Indeed, we have

$$\begin{aligned} -\left(\boldsymbol{\mathcal{F}}_j'[\mathbf{u}]\right)^T \boldsymbol{\psi}_{,j} + \mathcal{G}'[\mathbf{u}] - \left(\mathcal{G}'[\mathbf{u}_{,j}]\right)_{,j} = \mathbf{0}, \qquad \forall \boldsymbol{x} \in \Omega, \\ \left[\left(\boldsymbol{\mathcal{F}}_j'[\mathbf{u}]\right)^T \boldsymbol{\psi} + \mathcal{G}'[\mathbf{u}_{,j}]\right] \hat{n}_j = \mathbf{0}, \qquad \forall \boldsymbol{x} \in \Gamma_{\text{out}}. \end{aligned} \tag{13}$$

3.1. Variational multiscale formulation

For the finite-dimensional problem, we consider the following generic residual-based variational multiscale formulation of (8): find $\mathbf{u}^h \in [\mathsf{V}^h]^m$ such that

$$\mathcal{R}_h(\mathbf{v}^h, \mathbf{u}^h) \equiv \mathcal{R}(\mathbf{v}^h, \tilde{\mathbf{u}}(\mathbf{u}^h)) = 0, \qquad \forall \mathbf{v}^h \in [\mathsf{V}^h]^m, \tag{14}$$

where $\tilde{\mathbf{u}}(\mathbf{u}^h)$ denotes an approximation to the infinite dimensional solution $\mathbf{u}$. We note that $\tilde{\mathbf{u}}$ is defined only on element interiors, and as a result the domain integral in the equation above is replaced by the sum of integrals over element interiors, and the integral over Γ_{out} is replaced by an integral over a surface that is in the interior of Ω and is arbitrarily close to Γ_{out} (see (18) for the definition). Similarly, we will see that it is convenient to define the discrete functional as

$$\mathcal{J}_h(\mathbf{u}^h) \equiv \mathcal{J}(\tilde{\mathbf{u}}(\mathbf{u}^h)), \tag{15}$$

where the integral is to be interpreted as a sum over element interiors as discussed above for $\mathcal{R}$.

Presently, we place only two restrictions on the operator $\tilde{\mathbf{u}}$:

1. the primal solution is invariant under the action of the operator, i.e. $\tilde{\mathbf{u}}(\mathbf{u}) = \mathbf{u}$, and;

[4] Henceforth, we omit the explicit dependence of the integrands on $\mathbf{u}$ and $\mathbf{u}_{,j}$ and only show which variable is used to define the Fréchet derivative.

2. the Fréchet derivative of $\tilde{\mathbf{u}}$ satisfies $\tilde{\mathbf{u}}'[\mathbf{u}]\mathbf{v}^h \in C^1(\Omega_e)$ for all $\mathbf{v}^h \in [\mathsf{V}^h]^m$ and Ω_e, where Ω_e denotes the interior of an arbitrary element e.

Note that the variational multiscale semilinear form is identical to the pure Galerkin case, (8), with $\mathbf{u}$ replaced with $\tilde{\mathbf{u}}(\mathbf{u}^h)$ and $\mathbf{v}$ replaced with $\mathbf{v}^h$. In fact, selecting $\tilde{\mathbf{u}} = \mathbf{u}^h$ recovers the Galerkin case, whereas selecting $\tilde{\mathbf{u}}(\mathbf{u}^h) = \mathbf{u}^h - \boldsymbol{\tau}(\mathbf{u}^h, \mathbf{g})\boldsymbol{\mathcal{N}}(\mathbf{u}^h)$ in the interior of elements yields a common form of the variational multiscale formulation [11]. Here, $\boldsymbol{\tau}(\mathbf{u}^h, \mathbf{g})$, which is the stabilization matrix, is a continuous function of the solution $\mathbf{u}^h$ and the metric tensor $\mathbf{g}$. The metric tensor is defined as $\mathbf{g} = \mathbf{F}^T\mathbf{F}$, where $F_{ij} = \xi_{i,x_j}$ is the Jacobian of the map of the coordinates in the physical domain to the coordinates in the parent element domain. For isoparametric elements this map has the same class of continuity as the shape functions used to represent the solution. In particular, for C^0 continuous shape functions this map is C^0 continuous and as a result $\mathbf{F}$ and $\mathbf{g}$, which involve derivatives of this map, are discontinuous across element boundaries. For C^1 continuous shape functions this map is C^1 continuous, and hence $\mathbf{F}$ and $\mathbf{g}$ are continuous across element boundaries. Thus the dependence on $\mathbf{g}$ will lead to a τ that is discontinuous across elements for C^0 continuous shape functions, and is continuous for C^1 (or higher-order) continuous shape functions.

Based on the discretizations (14) and (15), the discrete adjoint equation follows immediately from (5). In particular, the discrete adjoint $\boldsymbol{\psi}^h \in [\mathsf{V}^h]^m$ satisfies

$$\mathcal{J}'[\tilde{\mathbf{u}}](\tilde{\mathbf{u}}'[\mathbf{u}^h]\mathbf{v}^h) + \mathcal{R}'[\tilde{\mathbf{u}}](\boldsymbol{\psi}^h, \tilde{\mathbf{u}}'[\mathbf{u}^h]\mathbf{v}^h) = 0, \qquad \forall \mathbf{v}^h \in [\mathsf{V}^h]^m. \tag{16}$$

For adjoint consistency, we need to show that (16) is satisfied when $\mathbf{u}^h$ and $\boldsymbol{\psi}^h$ are replaced by $\mathbf{u}$ and $\boldsymbol{\psi}$, respectively. That is, for an adjoint consistent method

$$\mathcal{J}'[\mathbf{u}](\mathbf{z}^h) + \mathcal{R}'[\mathbf{u}](\boldsymbol{\psi}, \mathbf{z}^h) = 0, \qquad \forall \mathbf{z}^h \in [\mathsf{Z}^h]^m \equiv \left\{ \tilde{\mathbf{u}}'[\mathbf{u}]\mathbf{v}^h \mid \mathbf{v}^h \in [\mathsf{V}^h]^m \right\}.$$

We have introduced $\mathbf{z}^h$ and $[\mathsf{Z}^h]^m$ to keep the subsequent derivations compact. The expression above appears similar to the left-hand side of (3), the weak form of the adjoint PDE; however, the above will not vanish in general, because Z^h is not necessarily a subset of V. To proceed with the analysis, we make use of the definitions of $\mathcal{R}'$ and $\mathcal{J}'$:

$$\begin{aligned}
\mathcal{J}'[\mathbf{u}](\mathbf{z}^h) + \mathcal{R}'[\mathbf{u}](\boldsymbol{\psi}, \mathbf{z}^h) \equiv & \sum_e \left\{ \int_{\Omega_e} \mathcal{G}'[\mathbf{u}]\mathbf{z}^h \, d\Omega + \int_{\Omega_e} \mathcal{G}'[\mathbf{u}_{,j}]\mathbf{z}^h_{,j} \, d\Omega - \int_{\Omega_e} \boldsymbol{\psi}^T_{,j}\boldsymbol{\mathcal{F}}'_j[\mathbf{u}]\mathbf{z}^h \, d\Omega \right\} \\
& + \int_{\tilde{\Gamma}_{\text{out}}} \boldsymbol{\psi}^T \boldsymbol{\mathcal{F}}'_j[\mathbf{u}]\hat{n}_j \mathbf{z}^h \, d\Gamma \\
= & \sum_e \int_{\Omega_e} \left\{ \mathcal{G}'[\mathbf{u}] - \left(\mathcal{G}'[\mathbf{u}_{,j}]\right)_{,j} - \boldsymbol{\psi}^T_{,j}\boldsymbol{\mathcal{F}}'_j[\mathbf{u}] \right\} \mathbf{z}^h \, d\Omega \\
& + \int_{\tilde{\Gamma}_{\text{out}}} \left\{ \boldsymbol{\psi}^T \boldsymbol{\mathcal{F}}'_j[\mathbf{u}]\hat{n}_j + \mathcal{G}'[\mathbf{u}_{,j}]\hat{n}_j \right\} \mathbf{z}^h \, d\Gamma + \int_{\tilde{\Gamma}} \mathcal{G}'[\mathbf{u}_{,j}]\hat{n}_j [\![\mathbf{z}^h]\!] \, d\Gamma,
\end{aligned}$$

where $\tilde{\Gamma}$ denotes inter-element boundaries, and $\tilde{\Gamma}_{\text{out}}$ is described below. In arriving at the second line we have performed integration by parts on the integral containing $\mathbf{z}^h_{,j}$, recognizing that $\mathbf{z}^h$ is of class C^1 on element interiors. We have also used the compatibility condition (10). In the last sum over elements, we have introduced the standard jump operator

$$[\![u]\!] \equiv \lim_{t \to 0} \left\{ \mathbf{u}(\boldsymbol{x} + t\hat{\boldsymbol{n}}) - \mathbf{u}(\boldsymbol{x} - t\hat{\boldsymbol{n}}) \right\}. \tag{17}$$

The collection of points denoted by $\tilde{\Gamma}_{\text{out}}$ requires some explanation. Let

$$\Gamma_{\text{out}}^{-} \equiv \lim_{t \to 0^{-}} \{\boldsymbol{x} + t\hat{\boldsymbol{n}} | \boldsymbol{x} \in \Gamma_{\text{out}}\}. \tag{18}$$

Then $\tilde{\Gamma}_{\text{out}}$ is the set of points in Γ_{out}^{-} that do not lie on any inter-element facet. Finally, making use of the adjoint PDE and its boundary conditions (13) — and assuming that $\boldsymbol{\mathcal{F}}$, $\mathcal{G}$ and $\mathbf{u}$ are sufficiently smooth so that the boundary condition applies on $\tilde{\Gamma}_{\text{out}}$ — we find

$$\mathcal{J}'[\mathbf{u}](\mathbf{z}^h) + \mathcal{R}'[\mathbf{u}](\boldsymbol{\psi}, \mathbf{z}^h) = \int_{\tilde{\Gamma}} \mathcal{G}'[\mathbf{u}_{,j}] \hat{n}_j [\![\mathbf{z}^h]\!] \, d\Gamma. \tag{19}$$

The variational multiscale method will be adjoint consistent only if the sum on the right-hand-side vanishes. Below, we verify this condition for three implementations of RBVMS, thereby confirming that they are adjoint consistent.

RBVMS with a C^1 basis: When RBVMS is used with spectral or NURBS basis [15, 17, 18], we have $\tilde{\mathbf{u}}(\mathbf{u}^h) = \mathbf{u}^h - \boldsymbol{\tau}(\mathbf{u}^h, \mathbf{g})\boldsymbol{\mathcal{N}}(\mathbf{u}^h)$, where $\boldsymbol{\tau}(\mathbf{u}^h, \mathbf{g})$ is the stabilization matrix [11]. Consequently, since $\boldsymbol{\mathcal{N}}(\mathbf{u}) = \mathbf{0}$ we have

$$\mathbf{z}^h = \tilde{\mathbf{u}}'[\mathbf{u}]\mathbf{v}^h = \mathbf{v}^h - \boldsymbol{\tau}(\mathbf{u}, \mathbf{g})\boldsymbol{\mathcal{N}}'[\mathbf{u}]\mathbf{v}^h.$$

Now, since the test function is C^1 continuous, it follows that $\boldsymbol{\mathcal{N}}'[\mathbf{u}]\mathbf{v}^h$ is C^0 continuous. Further, since the basis functions are C^1 continuous, the metric tensor $\mathbf{g}$, and hence $\boldsymbol{\tau}(\mathbf{u}, \mathbf{g})$ is also C^0 continuous. Consequently $\mathbf{z}^h$ and the jump terms in (19) vanish. Thus, the dual-consistency condition is satisfied.

RBVMS with bubble functions: When RBVMS is used in conjunction with bubble functions, local problems that are confined to element interiors are solved to determine the fine scale solution $\mathbf{u}'$. These problems are driven by the interior element residual and use basis functions that vanish on element interiors. As a result the solution to this problem, that is $\mathbf{u}'$, is guaranteed to be zero on inter-element boundaries. In this case [12–14], we have $\tilde{\mathbf{u}}(\mathbf{u}^h) = \mathbf{u}^h + \mathbf{u}' = \mathbf{u}^h$ on element facets; therefore, it is easy to show that

$$\mathbf{z}^h = \tilde{\mathbf{u}}'[\mathbf{u}]\mathbf{v}^h = \mathbf{v}^h, \qquad \forall x \in \tilde{\Gamma}.$$

Again, the jump terms in (19) vanish and we have dual-consistency.

RBVMS with a C^0 basis [15, 19]: As with a C^1 basis, we have $\tilde{\mathbf{u}}(\mathbf{u}^h) = \mathbf{u}^h - \boldsymbol{\tau}(\mathbf{u}^h, \mathbf{g})\boldsymbol{\mathcal{N}}(\mathbf{u}^h)$; however, when the test functions are only continuous at element boundaries, $[\![\mathbf{z}^h]\!] \neq \mathbf{0}$, in general. This is because both $\boldsymbol{\mathcal{N}}'[\mathbf{u}]\mathbf{v}^h$ and $\boldsymbol{\tau}(\mathbf{u}, \mathbf{g})$ are discontinuous at inter-element boundaries. In this case, the sum on the right-hand-side of (19) vanishes only if $\mathcal{G}'[\mathbf{u}_{,j}]\hat{n}_j = 0$ on element facets. The orientation of the element facets can be arbitrary, so this condition requires

$$\mathcal{G}'[\mathbf{u}_{,j}] = 0.$$

That is, for dual consistency $\mathcal{G}$ can be a function of $\mathbf{u}$ only.

4. Second-order Scalar PDEs

In this section we consider a scalar elliptic PDE as a model problem. Elliptic PDEs arise in numerous applications including elasticity and steady viscous fluid flow. In conservative form, scalar elliptic PDEs can be written as

$$\mathcal{N}(u) \equiv \mathcal{F}_{i,i}(u, \nabla u) - f = 0, \tag{20}$$

where, as before, $\mathcal{N}(u)$ is the strong form of the residual, $f \in L^2(\Omega)$ is the external forcing, and $\mathcal{F}_i$ is the i^{th} component of a flux field over Ω. For simplicity, we assume homogeneous boundary conditions, so that the variational form of (20) reads, find $u \in \mathsf{V}_0 \equiv H_0^1(\Omega)$ such that

$$\mathcal{R}(v, u) \equiv -\int_\Omega v_{,i}\mathcal{F}_i(u, \nabla u)\, d\Omega - \int_\Omega v f\, d\Omega = 0, \qquad \forall v \in \mathsf{V}_0. \tag{21}$$

Unlike the function space considered for the first-order hyperbolic system, here we require the admissible functions to vanish on the boundary, i.e. strongly imposed boundary conditions. To define the dual problem, we again consider functionals of the form

$$\mathcal{J}(u) \equiv \int_\Omega \mathcal{G}(u, \nabla u)\, d\Omega. \tag{22}$$

Referring to (3), the adjoint variational problem corresponding to (21) and (22) is, find $\psi \in \mathsf{V}_0$ such that

$$\int_\Omega \left(\mathcal{G}'[u]v + \mathcal{G}'[u_{,j}]v_{,j}\right)\, d\Omega - \int_\Omega \psi_{,i}\left(\mathcal{F}_i'[u]v + \mathcal{F}_i'[u_{,j}]v_{,j}\right)\, d\Omega = 0, \qquad \forall v \in \mathsf{V}_0. \tag{23}$$

The strong form of the adjoint PDE can be found by applying integration by parts to isolate the test function v from the remaining terms. Recalling that the test functions v vanish on the domain boundary, we find that the adjoint PDE is

$$\mathcal{G}'[u] - (\mathcal{G}'[u_{,j}])_{,j} - \mathcal{F}_i'[u]\psi_{,i} + \left(\mathcal{F}_i'[u_{,j}]\psi_{,i}\right)_{,j} = 0, \tag{24}$$

where, like the primal solution, ψ also satisfies homogeneous Dirichlet boundary conditions. Sufficiently smooth adjoint solutions ψ will satisfy the above strong form of the adjoint PDE, and this fact will be used below.

4.1. Variational Multiscale Formulation

Consider a generic variational-multiscale discretization of (21): find $u_h \in \mathsf{V}_0^h$ such that

$$\mathcal{R}_h(v^h, u^h) \equiv \mathcal{R}(v^h, \tilde{u}(u^h)) = 0, \qquad \forall v^h \in \mathsf{V}_0^h. \tag{25}$$

As before, $\tilde{u}$ is defined only over element interiors, and the only restrictions placed on the operator $\tilde{u}$ are that $\tilde{u}(u) = u$ and $\tilde{u}'[u]v^h \in C^1(\Omega_e)$. The discretized functional is given by

$$\mathcal{J}_h(u^h) \equiv \mathcal{J}(\tilde{u}(u^h)). \tag{26}$$

We note that any integral involving $\tilde{u}$ must be interpreted as a sum of integrals over element interiors since $\tilde{u}$ is not defined on element boundaries. The discrete adjoint, $\psi^h \in \mathsf{V}_0^h$, for the elliptic problem satisfies

$$\mathcal{J}'[\tilde{u}](\tilde{u}'[u^h]v^h) + \mathcal{R}'[\tilde{u}](\psi^h, \tilde{u}'[u^h]v^h) = 0, \qquad \forall v^h \in \mathsf{V}_0^h. \tag{27}$$

Replacing u^h and ψ^h above by u and ψ, respectively, we find the following condition must be satisfied in order to ensure adjoint consistency.

$$\mathcal{J}'[u](z^h) + \mathcal{R}'[u](\psi, z^h) = 0, \qquad \forall z^h \in \mathsf{Z}_0^h \equiv \left\{ \tilde{u}'[u]v^h \mid v^h \in \mathsf{V}_0^h \right\}.$$

Next, we introduce the semilinear form defined in (21) and the functional (26). We find

$$\begin{aligned}
&\mathcal{J}'[u](z^h) + \mathcal{R}'[u](\psi, z^h) \\
&\qquad = \sum_e \left\{ \int_{\Omega_e} \left(\mathcal{G}'[u]z^h + \mathcal{G}'[u_{,j}]z^h_{,j} \right) d\Omega - \int_{\Omega_e} \psi_{,i} \left(\mathcal{F}_i'[u]z^h + \mathcal{F}_i'[u_{,j}]z^h_{,j} \right) d\Omega \right\},
\end{aligned}$$

where the sum is over all elements. We now follow the same process used for the hyperbolic case. We use the assumption that z^h is of class C^1 on element interiors, so that we can apply integration by parts element-wise to isolate the strong form of the adjoint PDE. The integral containing the adjoint residual then vanishes (for sufficiently smooth ψ) and we are left with

$$\begin{aligned}
\mathcal{J}'[u](z^h) + \mathcal{R}'[u](\psi, z^h) = &\int_{\tilde{\Gamma}} \left(\mathcal{G}'[u_{,j}] - \psi_{,i}\mathcal{F}_i'[u_{,j}] \right) \hat{n}_j [\![z^h]\!] \, d\Gamma \\
&+ \int_{\tilde{\Gamma}_{\text{bnd}}} \left(\mathcal{G}'[u_{,j}] - \psi_{,i}\mathcal{F}_i'[u_{,j}] \right) \hat{n}_j z^h \, d\Gamma,
\end{aligned} \tag{28}$$

where, as before, $\tilde{\Gamma}$ denotes inter-element boundaries. The set denoted by $\tilde{\Gamma}_{\text{bnd}}$ is interior to the domain Ω and is defined by

$$\tilde{\Gamma}_{\text{bnd}} \equiv \lim_{t \to 0^-} \{ \mathbf{x} + t\hat{\mathbf{n}} | \mathbf{x} \in \Gamma \} \setminus \tilde{\Gamma}$$

The variational multiscale method will be adjoint consistent only if the two integrals on the right-hand-side of (28) vanish. We list two implementations for which this is the case.

RBVMS with a C^2 basis: Suppose we use residual-based variational-multiscale stabilization with a C^m basis, where $m \geq 2$; e.g., cubic B-splines, or with a spectral basis. Then

$$z^h = \tilde{u}'[u]v^h = v^h - \tau(u, \mathbf{g})\mathcal{N}'[u]v^h. \tag{29}$$

In this case, $\mathcal{N}'[u]v^h$ is continuous over element facets, because the second-derivative operator in $\mathcal{N}'[u]$ is applied to a test function that is at least C^2 continuous. Also the metric tensor $\mathbf{g}$ and hence the stabilization parameter $\tau(u)$ are continuous over element facets because the basis functions are C^2 continuous. Thus, the integral over the inter-element facets on the right-hand-side of (28) vanishes. To ensure that the integral over $\tilde{\Gamma}_{\text{bnd}}$ is zero, z^h must be made to vanish on this set. There are a number of strategies that can be used to accomplish this, such as forcing $\tau(u, \mathbf{g})$ to vanish on the boundary; an alternative approach is taken in the numerical example presented below. Regardless of the approach taken, if z^h vanishes on $\tilde{\Gamma}_{\text{bnd}}$ then both integrals on the right-hand-side of (28) are zero, and the scheme based on the C^2 basis is adjoint consistent.

RBVMS with bubble functions: If bubble functions are used to define the fine space, then on element facets and $\tilde{\Gamma}_{\text{bnd}}$ we have $\tilde{u}(u^h) - u^h = 0$, and, consequently, $z^h = v^h$. It follows that RBVMS based on bubble functions is adjoint consistent for the elliptic problem.

In contrast with the hyperbolic case, RBVMS based on C^0 elements is not adjoint consistent for elliptic problems, at least when using the standard definition[5].

5. Numerical Examples

The numerical examples presented below focus on the role of adjoint consistency on functional superconvergence. These examples demonstrate that adjoint-consistent RBVMS schemes are useful even when the adjoint is not explicitly computed. As discussed in the introduction, there are other applications (e.g. optimal control, a posteriori error estimation and adaptation) for which adjoint consistency also plays a role, but these are not considered here.

5.1. Inviscid Burgers with Gradient-based Functional

Our first numerical example illustrates the impact of adjoint consistency on a functional that depends on the solution of a first-order PDE. Consider the steady inviscid Burgers equation on the unit interval:

$$\begin{aligned} \frac{\partial u^2}{\partial x} - f = 0, \qquad \forall x \in [0,1], \\ u(0) - u_L = 0. \end{aligned} \tag{30}$$

The source term f and boundary condition u_L are determined by fixing the exact solution to be

$$u(x) = 1 + x \sin(4\pi x).$$

Our nonlinear functional of interest is

$$\mathcal{J}(u) = \int_0^1 \left(\frac{\partial u}{\partial x}\right)^2 dx. \tag{31}$$

The integrand for $\mathcal{J}$ depends on the gradient of u, so the conditions for adjoint consistency described at the end of Section 5.1 are not satisfied for a C^0 basis.

The finite-element formulation of (30) with residual-based variational multiscale stabilization and weakly imposed boundary conditions yields the following discrete problem: find $u^h \in \mathsf{V}^h$ such that

$$-\int_0^1 \tilde{u}(u^h)^2 \frac{\partial v^h}{\partial x}\, dx + \left(v^h \left(\tilde{u}(u^h)\right)^2\right)\Big|_{x=1} - \left(v^h u_L^2\right)\Big|_{x=0} - \int_0^1 f v^h\, dx = 0, \qquad \forall v^h \in \mathsf{V}^h,$$

where

$$\tilde{u}(u^h) = u^h - \tau(u^h, g)\left(\frac{\partial (u^h)^2}{\partial x} - f\right), \qquad \text{and} \qquad \tau(u^h, g) = \frac{h}{2|u^h|}.$$

Element size is defined as $h = 2/\sqrt{g}$, where $g = \xi_x^2$ here. The space V^h corresponds to continuous Lagrange elements on a mesh of n elements. The mesh has uniform element sizes of $h(x) = 2/n$ for $x < 0.5$ and $h(x) = 2/(3n)$ for $x > 0.5$. The nonsmooth mesh spacing is chosen to prevent the

[5] Carefully chosen jump terms can be introduced into the standard $\tilde{u}$ definition such that $[\![z^h]\!]$ vanishes; however, similar to edge-based stabilizations [21, 22], the jump terms couple adjacent elements and increase the stencil size.

occurrence of error cancellations that sometimes appear on grids with uniform spacing. Finally, the exact value of $\mathcal{J}$ is approximated by integrating the exact gradient on a mesh consisting of 4800 eighth-degree elements. All calculations are performed using the FEniCS suite of tools [23].

Figure 1(a) shows the L^2 errors of the solution for 33 mesh sizes, defined by $n \in \{32 + 4\,i\}_{i=0}^{32}$. The nominal mesh spacing in Figure 1(a), as well as the following figures, is given by $h = 1/n$. On the coarsest grids, the L^2 errors exhibit $(p+2)$-order convergence rates, but these rates decrease with refinement. On the finest set of grids, the errors for the linear elements have the expected $(p+1)$-order asymptotic convergence rate, while the L^2 errors for the $p = 2$ and $p = 3$ cases have rates between $p + 1$ and $p + 2$.

Figure 1(b) plots the functional error for the same 33 grids and polynomial orders. The gradient in the integrand of $\mathcal{J}$ is found by differentiating u^h; thus, based on the theory presented in Section for C^0 elements, we expect the functional to exhibit suboptimal convergence rates. Indeed, for $p = 2$ and $p = 3$, the functionals converge at a rate of $p + 1$, i.e. the same asymptotic rate as the L^2 error. The linear elements appear to exhibit superconvergence, but this is true only over the range of h plotted; for sufficiently small mesh spacing the $p = 1$ errors also have a suboptimal convergence rate.

The conditions for adjoint consistency can easily be recovered in the present example by performing an L^2 projection of the gradient. In fact, this technique will recover superconvergence for any gradient-based functional when the solution depends on a first-order PDE. Projecting the gradient is equivalent to writing a first-order system for the solution and gradient, where the solution is decoupled from the gradient in the case of a first-order PDE. Thus, rather than using $\partial u^h/\partial x$ in the functional, we use $w^h \in \mathsf{V}^h$ such that

$$\int_0^1 w^h v^h \, dx + \int_0^1 \tilde{u}(u^h) \frac{\partial v^h}{\partial x} \, dx - \left(v^h \tilde{u}(u^h) \right) \Big|_{x=1} + \left(v^h u_L \right) \Big|_{x=0} = 0, \qquad \forall v^h \in \mathsf{V}^h.$$

Notice that w^h corresponds to the projected gradient of $\tilde{u}(u^h)$ and not u^h. This is consistent with the definition of an RBVMS residual for a first-order system, and ignoring this definition does impact adjoint consistency: Figure 1(c) shows the functional error when w^h is the projected gradient of u^h. Compared with the unprojected-gradient results, the projected gradient has little impact on the asymptotic convergence rate of the functional for the $p = 2$ and $p = 3$ cases. For the $p = 1$ case, the projected gradient actually increases the error and reduces the rate over the range of mesh sizes considered.

In contrast, Figure 1(c) shows the functional error when w^h is the projected gradient of $\tilde{u}(u^h)$. Note the change in the y-axis range from the previous results. Here, because the conditions for adjoint consistency are met, we observe the optimal superconvergent rate of $2(p+1) - m = 2p+1$, where m is the order of the highest derivative operator in the PDE; see, for example, [3].

We conclude this section by remarking that a projected gradient can also be used to achieve adjoint consistency for RBVMS discretizations of second-order PDEs on C^0 finite elements, i.e. rewrite the second-order PDE as a first-order system. Of course, the solution is not decoupled from the gradient in this case, and the gradient computation is no longer a simple post-processing step.

5.2. Linear Advection Diffusion

For our second numerical example, we consider the linear advection-diffusion equation and investigate the role of basis continuity on functional superconvergence. The differential equation

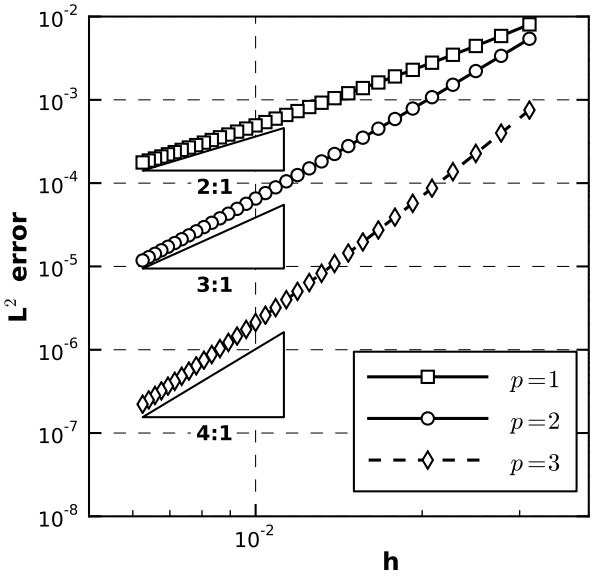

(a) L^2 error

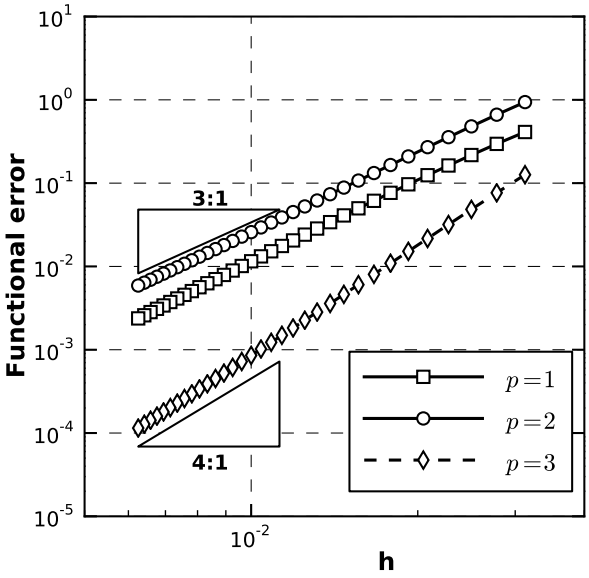

(b) functional error (no projection)

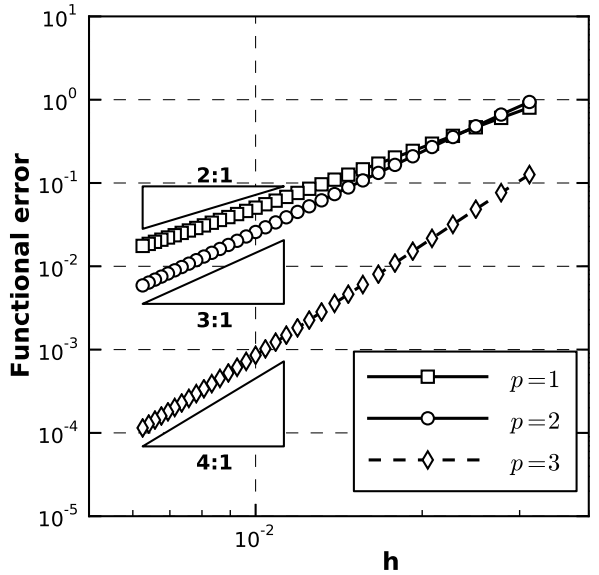

(c) functional error (projected gradient of u^h)

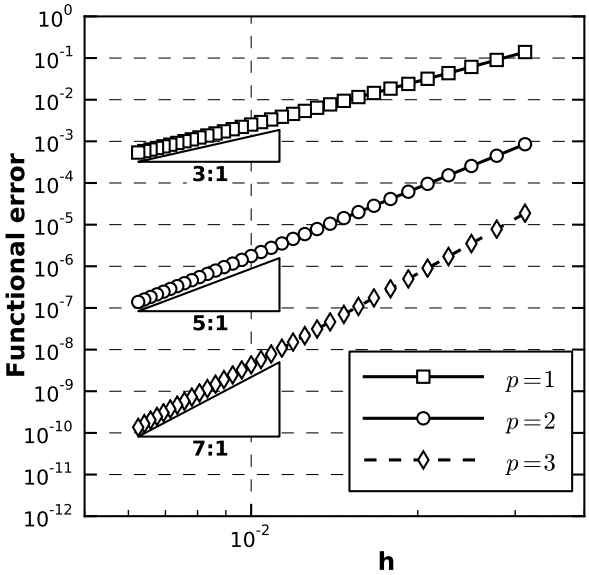

(d) functional error (projected gradient of $\tilde{u}$)

Figure 1: L^2 solution errors and functional errors for the inviscid Burgers example.

and boundary conditions are given by

$$\begin{aligned} &\frac{\partial u}{\partial x} - \epsilon \frac{\partial^2 u}{\partial x^2} = 0 \qquad \forall x \in [0,1], \\ &u(0) = 0, \qquad \text{and} \qquad u(1) = 1, \end{aligned} \tag{32}$$

where the diffusion coefficient is the constant $\epsilon = 0.1$. The exact solution is

$$u(x) = \frac{1 - e^{\frac{x}{\epsilon}}}{1 - e^{\frac{1}{\epsilon}}},$$

and the functional for this study is

$$\mathcal{J}(u) = \int_0^1 u^2 \, dx.$$

The second-order differential equation (32) is discretized using RBVMS-stabilized finite-elements with strongly imposed boundary conditions. Formally, the discrete solution $u^h \in \mathsf{V}^h$ satisfies

$$-\int_0^1 \tilde{u}(u^h) \frac{\partial v^h}{\partial x} \, dx + \epsilon \int_0^1 \frac{\partial \tilde{u}(u^h)}{\partial x} \frac{\partial v^h}{\partial x} \, dx = 0, \qquad \forall v^h \in \mathsf{V}_0^h.$$

For the trail space, V^h, we consider both C^0 cubic elements and C^2 cubic splines. The spline basis is constructed using uniform knot spacing and end knots of multiplicity 4, so that the basis interpolates at the boundary nodes. For both the C^0 and C^2 cases, the test space, V_0^h, is constrained to vanish on the boundary. For further details on the C^2 finite-element discretization see [24] and [25]

For all the elements of the C^0 discretization, as well as the interior elements of the C^2 discretization (i.e. elements whose facets do not overlap with the boundary), the operator $\tilde{u}(u^h)$ takes the form

$$\tilde{u}(u^h) = u^h - \tau(u^h, g) \left(\frac{\partial u^h}{\partial x} - \epsilon \frac{\partial^2 u^h}{\partial x^2} \right), \tag{33}$$

where

$$\tau(u^h, g) = \frac{h}{2} \min\left(1, \frac{\mathrm{Pe}}{3p^2}\right), \qquad \text{and} \qquad \mathrm{Pe} = \frac{h}{2\epsilon}.$$

The polynomial order is $p = 3$ for all cases considered. As with the Burgers example, $h = 2/\sqrt{g}$.

For the elements adjacent the boundary, we consider two options for the definition of $\tilde{u}(u^h)$ in the C^2 discretization. The first option is to use the definition given above for both the interior and boundary-adjacent elements. This is the approach commonly used in RBVMS implementations. For the second option, $\tilde{u}(u^h)$ is modified such that it coincides with u^h at the boundary. To be precise, consider the element at the left boundary, $\Omega_1 = \{0 \leq x \leq x_1\}$, where x_1 is the node/knot defining the facet between the first and second elements. In the reference space $\xi \in [-1, 1]$, we have

$$\tilde{u}(u^h) = u^h + \frac{\xi + 1}{2} u^*, \tag{34}$$

where u^* is a constant over the first element and is defined by

$$u^* = \lim_{t \to 0^+} \left[-\tau(u^h, g) \left(\frac{\partial u_h}{\partial x} - \epsilon \frac{\partial^2 u^h}{\partial x^2} \right) \right]_{x_1 + t}.$$

In other words, $(\xi + 1)u^*/2$ is a linear function that vanishes at the boundary $x = 0$ and ensures continuity of z^h at the interface between the first and second elements. An analogous modification is adopted at the element adjacent the $x = 1$ boundary. The motivation for these boundary-element modifications is the integral over $\tilde{\Gamma}_{\text{bnd}}$ in (28). The definition (34) and its analog over the right-boundary element ensure that $\tilde{u}(u^h) - u^h = 0$ on the boundary, which is necessary for adjoint consistency.

For the convergence study we consider a set of 7 grids with elements of uniform width. The number of elements or knot intervals is $n \in \{5 \times 2^i\}_{i=0}^6$. The functional error is defined as $|\mathcal{J}(u) - \mathcal{J}(\tilde{u}(u^h))|$.

Figure 2(a) plots the L^2 and functional errors for the C^0 RBVMS discretization of the advection-diffusion equation. Both errors are asymptotically fourth order. The absence of functional superconvergence is consistent with the present theory, which concludes that RBVMS stabilization of second-order PDEs is not adjoint consistent with C^0 elements.

The results for the C^2 discretization, with $\tilde{u}(u^h)$ based on (33) *for all elements*, are plotted in Figure 2(b). Again, no functional superconvergence is observed. This is also anticipated by the present theory, which requires that z^h vanish at the boundary for adjoint consistency of second-order PDEs.

Finally, Figure 2(c) shows the C^2-discretization results when the boundary elements use the modified $\tilde{u}(u^h)$ definition; see (34) for the left-boundary modification. As discussed above, this modified definition ensures that z^h vanishes at the boundaries and has negligible impact on the solution error; however, the modification produces an adjoint-consistent C^2 discretization, and the impact on functional accuracy is obvious. We observe a superconvergent rate of $2(p + 1) - m = 2p = 6$. The functional error on the finest grid shows some degradation due to round-off errors.

6. Conclusions

Adjoint consistency improves integral functional convergence rates and solution convergence in the L^2 norm. In addition, the discrete adjoint variables of an adjoint consistent scheme offer advantages for optimal control problems and output-based adaptation.

We have shown that some variational multiscale formulations are adjoint consistent for a model hyperbolic and elliptic equation. In particular, RBVMS based on bubble functions is adjoint consistent for both types of PDEs. More generally, RBVMS is adjoint consistent if a C^1 basis is used for the hyperbolic equation or a C^2 basis is used for the elliptic equation in conjunction with subgrid scales that vanish on Dirichlet boundaries.

When a C^0 continuous finite-element space is adopted, RBVMS will produce an adjoint consistent discretization of the hyperbolic system, provided the functional integrand does not depend on the solution gradient. In contrast, we have shown that the elliptic equation is not adjoint consistent when discretized using a C^0 basis.

[1] Gunzburger, M. D., *Perspectives in flow control and optimization*, Society for Industrial and Applied Mathematics, 2003.

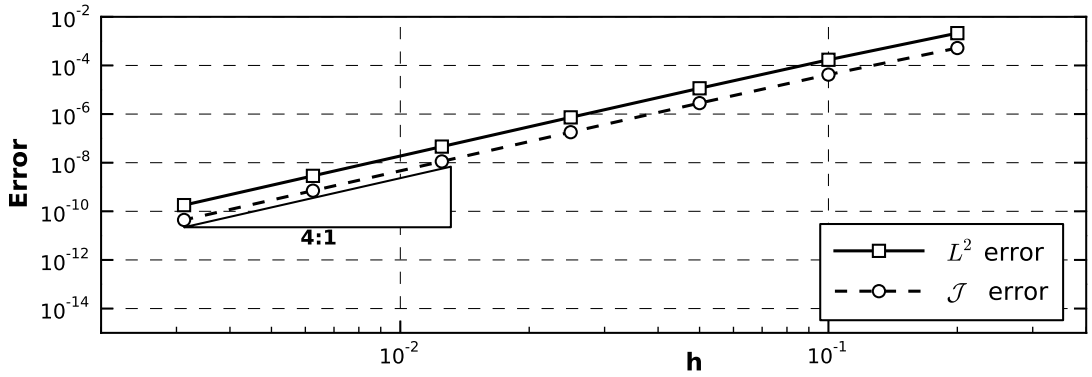

(a) C^0 elements

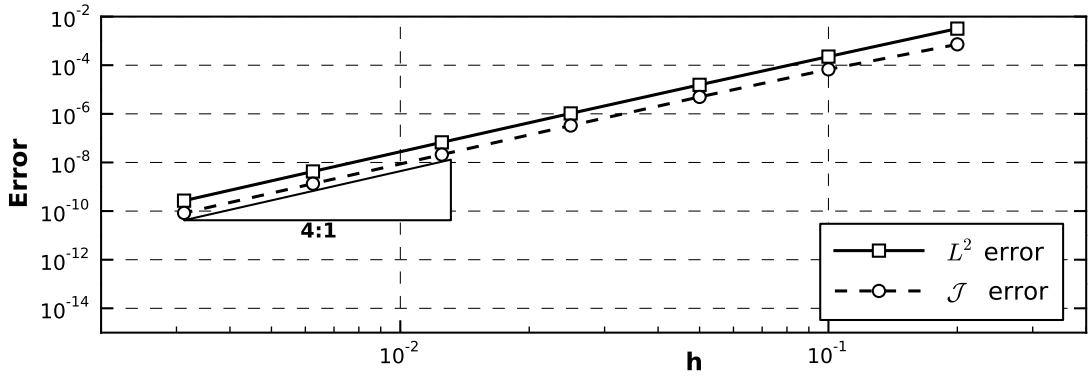

(b) C^2 elements without boundary modification of $\tilde{u}(u^h)$

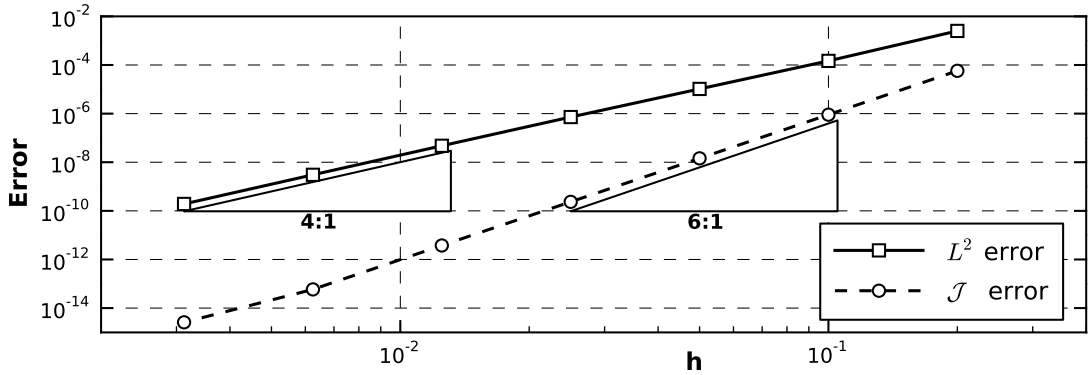

(c) C^2 elements with boundary modification of $\tilde{u}(u^h)$

Figure 2: L^2 solution errors and functional errors for the linear advection-diffusion example.

[2] Arnold, D. N., Brezzi, F., Cockburn, B., and Marini, L. D., "Unified Analysis of Discontinuous Galerkin Methods for Elliptic Problems," *SIAM Journal on Numerical Analysis*, Vol. 39, No. 5, 2002, pp. 1749–1779.

[3] Pierce, N. A. and Giles, M. B., "Adjoint recovery of superconvergent functionals from PDE approximations," *SIAM Review*, Vol. 42, No. 2, 2000, pp. 247–264.

[4] Lu, J. C., *An a posteriori error control framework for adaptive precision optimization using discontinuous Galerkin finite element method*, Ph.D. thesis, Massachusetts Institute of Technology, Cambridge, Massachusetts, 2005.

[5] Griewank, A., *Evaluating Derivatives*, SIAM, Philadelphia, PA, 2000.

[6] Houston, P., Rannacher, R., and Süli, E., "A posteriori error analysis for stabilised finite element approximations of transport problems," *Computer Methods in Applied Mechanics and Engineering*, Vol. 190, No. 11-12, Dec. 2000, pp. 1483–1508.

[7] Hartmann, R., "Adjoint Consistency Analysis of Discontinuous Galerkin Discretizations," *SIAM Journal on Numerical Analysis*, Vol. 45, No. 6, 2007, pp. 2671–2696.

[8] Braack, M., "Optimal Control in Fluid Mechanics by Finite Elements with Symmetric Stabilization," *SIAM Journal on Control and Optimization*, Vol. 48, No. 2, Jan. 2009, pp. 672–687.

[9] Hicken, J. E. and Zingg, D. W., "The role of dual consistency in functional accuracy: error estimation and superconvergence," *20th AIAA Computational Fluid Dynamics Conference*, No. AIAA-2011-3855, Honolulu, Hawaii, United States, June 2011.

[10] Hicken, J. E. and Zingg, D. W., "Dual consistency and functional accuracy: a finite-difference perspective," submitted to JCP, 2012.

[11] Hughes, T. J. R., "Multiscale Phenomena: Green's Functions, the Dirichlet-to-Neumann Formulation, Subgrid Scale Models, Bubbles and the Origins of Stabilized Methods," *Computer Methods in Applied Mechanics and Engineering*, Vol. 127, 1995, pp. 387–401.

[12] Franca, L. P. and Russo, A., "Deriving upwinding, mass lumping and selective reduced integration by residual-free bubbles," *Applied Mathematics Letters*, Vol. 9, No. 5, Sept. 1996, pp. 83–88.

[13] Oberai, A. A. and Pinsky, P. M., "A multiscale finite element method for the Helmholtz equation," *Computer Methods in Applied Mechanics and Engineering*, Vol. 154, No. 3-4, March 1998, pp. 281–297.

[14] Masud, A. and Khurram, R. A., "A multiscale/stabilized finite element method for the advectiondiffusion equation," *Computer Methods in Applied Mechanics and Engineering*, Vol. 193, No. 21-22, May 2004, pp. 1997–2018.

[15] Bazilevs, Y., Calo, V. M., Cottrell, J. A., Hughes, T. J. R., Reali, A., and Scovazzi, G., "Variational multiscale residual-based turbulence modeling for large eddy simulation of incompressible flows," *Computer Methods in Applied Mechanics and Engineering*, Vol. 197, No. 1-4, Dec. 2007, pp. 173–201.

[16] Hughes, T. J. R. and Sangalli, G., "Variational Multiscale Analysis: the Finescale Green's Function, Projection, Optimization, Localization, and Stabilized Methods," *SIAM Journal on Numerical Analysis*, Vol. 45, No. 2, Jan. 2007, pp. 539–557.

[17] Akkerman, I., Bazilevs, Y., Calo, V. M., Hughes, T. J. R., and Hulshoff, S., "The role of continuity in residual-based variational multiscale modeling of turbulence," *Computational Mechanics*, Vol. 41, No. 3, Feb. 2008, pp. 371–378.

[18] Wang, Z. and Oberai, A. A., "A mixed large eddy simulation model based on the residual-based variational multiscale formulation," *Physics of Fluids*, Vol. 22, No. 7, 2010, pp. 1–9.

[19] Gamnitzer, P., Gravemeier, V., and Wall, W. A., "Time-dependent subgrid scales in residual-based large eddy simulation of turbulent channel flow," *Computer Methods in Applied Mechanics and Engineering*, Vol. 199, No. 13-16, Feb. 2010, pp. 819–827.

[20] Hartmann, R., "Error estimation and adjoint based refinement for an adjoint consistent DG discretization of the compressible Euler equations," *International Journal of Computing Science and Mathematics*, Vol. 1, No. 2–4, 2007, pp. 207–220.

[21] Douglas, J. and Dupont, T., "Interior Penalty Procedures for Elliptic and Parabolic Galerkin Methods Computing Methods in Applied Sciences," *Computing Methods in Applied Sciences*, edited by R. Glowinski and J. L. Lions, Vol. 58 of *Lecture Notes in Physics*, chap. 6, Springer Berlin / Heidelberg, Berlin, Heidelberg, 1976, pp. 207–216.

[22] Burman, E., Fernández, M. A., and Hansbo, P., "Continuous Interior Penalty Finite Element Method for Oseen's Equations," *SIAM Journal on Numerical Analysis*, Vol. 44, No. 3, 2006, pp. 1248–1274.

[23] Logg, A., Mardal, K.-A., and Wells, G., editors, *Automated Solution of Differential Equations by the Finite Element Method*, Vol. 84, Springer Berlin Heidelberg, Berlin, Heidelberg, 2012.

[24] Bazilevs, Y. and Hughes, T. J. R., "Weak imposition of Dirichlet boundary conditions in fluid mechanics,"

Computers & Fluids, Vol. 36, No. 1, Jan. 2007, pp. 12–26.

[25] Borden, M. J., Scott, M. A., Evans, J. A., and Hughes, T. J. R., "Isogeometric finite element data structures based on Bézier extraction of NURBS," *Int. J. Numer. Meth. Engng.*, Vol. 87, No. 1-5, July 2011, pp. 15–47.